High-Resolution SAR Interferometry: Estimation of Local Frequencies in the Context of Alpine Glaciers

Gabriel Vasile, *Member, IEEE*, Emmanuel Trouvé, *Member, IEEE*, Ivan Petillot, Philippe Bolon, *Member, IEEE*, Jean-Marie Nicolas, Michel Gay, Jocelyn Chanussot, *Senior Member, IEEE*, Tania Landes, Pierre Grussenmeyer, Vasile Buzuloiu, *Senior Member, IEEE*, Irena Hajnsek, Christian Andres, Martin Keller, and Ralf Horn

Abstract—Synthetic aperture radar (SAR) interferometric data offer the opportunity to measure temperate glacier surface topography and displacement. The increase of the resolution provided by the most recent SAR systems has some critical implications. For instance, a reliable estimate of the phase gradient can only be achieved by using interferogram local frequencies. In this paper, an original two-step method for estimating local frequencies is proposed. The 2-D phase signal is considered to have two deterministic components corresponding to low-resolution (LR) fringes and high-resolution (HR) patterns due to the local microrelief, respectively. The first step of the proposed algorithm consists in the LR phase flattening. In the second step, the local HR frequencies are estimated from the phase 2-D autocorrelation function computed on adaptive neighborhoods. This neighborhood is the set of connected pixels belonging to the same HR spatial feature and respecting the "local stationarity" hypothesis. Results with both simulated TerraSAR-X interferograms and real airborne E-SAR images are presented to illustrate the potential of the proposed method.

Index Terms—Adaptive neighborhood, Experimental synthetic aperture radar (E-SAR), glacier monitoring, local frequencies, SAR interferometry (InSAR), TerraSAR-X.

I. INTRODUCTION

WITH an increased resolution, new spaceborne synthetic aperture radar (SAR) images will be an important source of information for the monitoring of glacier activity, by providing regular measurements such as surface topography, velocity fields or rocks, and crevasse cartography. After successful SAR experiments on Arctic and polar region glaciers [1], the study of Alpine temperate glaciers proved to be more complex. Some experiments carried out with existing spaceborne interferometric SAR (InSAR) data have shown that only specific data such as European Remote Sensing satellite (ERS) 1/2 tandem couples provide information on well-oriented glaciers at certain times of the year [2]. However, the characteristics of future spaceborne SAR missions such as TerraSAR-X (11-day repeat cycle, left/right looking, various incidence angles, up to 2-m resolution, dual polarization, etc.) reinforce the potential of interferometric measurements over Alpine glaciers.

The existing standard interferometric processing chains such as the differential interferometric automated process applied to survey of nature (DIAPASON) [3] or the repeated orbit interferometry package (ROI-PAC) [4], [5] provide a complete D-InSAR processing chain. These algorithms have already been tested and successfully applied in the context of SAR interferometry to measure accurate displacements (volcanology or seismology). These processors are built from standard well-established InSAR algorithms such as coregistration of single-look complex (SLC) images, phase scaling, and unwrapping. However, this procedure is often error prone when applied to temperate glacier monitoring because of the complex glacier topography (Fig. 1) or the phase noise and discontinuities at glacier boundaries.

With decameter resolution (about 20 m for ERS SAR images), the amplitude is often difficult to use to extract precise information. Different methods have been developed to derive ice velocity measurement, either by "speckle tracking" [6], [7] or by feature tracking [8]. These methods should benefit from the new generation of SAR satellites with meter resolution

G. Vasile was with the Laboratoire d'Informatique, Systèmes, Traitement de l'Information et de la Connaissance, Université de Savoie, Polytech'Savoie, BP 80439, 74944 Annecy-le-vieux Cedex, France, Laboratoire Grenoble Images Parole Signal Automatique, Centre National de la Recherche Scientifique (CNRS), Institut National Polytechnique de Grenoble, 46-38402 Saint-Martin-d'Hères Cedex, France, and also with the Laboratorul de Analiza si Prelucrarea Imaginilor, Universitatea Politehnica Bucuresti, 060032 Bucharest, Romania (e-mail: gabriel.vasile@univ-savoie.fr)

E. Trouvé is with the Laboratoire d'Informatique, Systèmes, Traitement de l'Information et de la Connaissance, Université de Savoie, Polytech'Savoie, 74944 Annecy-le-vieux Cedex, France, and was also with the Laboratoire Grenoble Images Parole Signal Automatique, CNRS, Institut National Polytechnique de Grenoble, BP 46-38402 Saint-Martin-d'Hères Cedex, France (e-mail: emmanuel.trouve@univ-savoie.fr).

I. Petillot and P. Bolon are with the Laboratoire d'Informatique, Systèmes, Traitement de l'Information et de la Connaissance, Université de Savoie, Polytech'Savoie, 74944 Annecy-le-vieux Cedex, France (e-mail: ivan.petillot@univ-savoie.fr; philippe.bolon@univ-savoie.fr).

J.-M. Nicolas is with the Département Traitement du Signal et des Images, CNRS, Ecole Nationale Supérieure des Télécommunications, 75013 Paris, France (e-mail: nicolas@tsi.enst.fr).

M. Gay and J. Chanussot are with the Laboratoire Grenoble Images Parole Signal Automatique, CNRS, Institut National Polytechnique de Grenoble, BP 46-38402 Saint-Martin-d'Hères cedex, France (e-mail: michel.gay@gipsa-lab.inpg.fr; jocelyn.chanussot@gipsa-lab.inpg.fr).

T. Landes and P. Grussenmeyer are with the Equipe Photogrammétrie et Géomatique, CNRS, Institut National des Sciences Appliquées de Strasbourg, 67084 Strasbourg Cedex, France (e-mail: tania.landes@insa-strasbourg.fr; pierre.grussenmeyer@insa-strasbourg.fr).

V. Buzuloiu is with the Laboratorul de Analiza si Prelucrarea Imaginilor, Universitatea Politehnica Bucuresti, 060042 Bucuresti, Romania (e-mail: buzuloiu@alpha.imag.pub.ro).

I. Hajnsek, C. Andres, M. Keller, and R. Horn are with the German Aerospace Center, Microwaves and Radar Institute, SAR Technology Department, 82234 Wessling, Germany (e-mail: irena.hajnsek@dlr.de; christian.andres@dlr.de; martin.keller@dlr.de; ralf.horn@dlr.de).

Color versions of one or more of the figures in this paper are available online at http://ieeexplore.ieee.org.

Digital Object Identifier 10.1109/TGRS.2007.912713

Fig. 1. May 2004: Surface topography and texture variability on the Mer-de-glace glacier (human size marked in red).

images and fully polarimetric data. This should allow to detect different features, to identify backscattering mechanisms, and to improve the extraction of the geometric deterministic component of the interferometric phase by adaptive techniques [9], [10] or multiresolution approaches [11], [12].

InSAR measurements include topographic fringes (phase variations due to the relief), which are useful in estimating the surface elevation for deriving glacier volume change [13], and displacement fringes (induced by the glacier displacement between the two InSAR acquisitions), which are useful in estimating ice stain rates [14]. The main limitations are

- temporal decorrelation due to glacier surface and subsurface fast changes, particularly during the warmest season [15];
- volume decorrelation caused by microwave penetration into uniform ice and associated elevation bias for topographic measurements [16];
- the need to separate the topographic fringes from the displacement fringes and possible atmospheric perturbations [17].

To estimate the surface displacement, one of the safest options consists in using an external digital terrain model (DTM) of the target area. However, the required accuracy of the DTM increases with the baseline between the two SAR acquisitions, making interferograms more and more sensitive to the topography. This is particularly crucial in the regions presenting deeply embedded valleys such as the glacial valleys in the Alps.

In this context, reliable estimates of the phase gradient within the interferogram become more and more necessary as the resolution of SAR data increases: smaller ground resolution cells will reveal the local topographic variations (microrelief), and larger baselines (smaller altitude of ambiguity) will transform them into local fringe pattern. These fringes are difficult to detect without using locally adaptive techniques. Previous approaches based on the estimation of local frequencies proved to be rather efficient with low-resolution (LR) data [11], [18]. If correctly estimated, local frequencies can be used in the InSAR processing at different stages, such as interferogram filtering [19] or phase unwrapping [20]–[22]. They are also used for

accurate coherence estimation obtained by compensating the local phase slope to avoid the bias (underestimation) due to the phase rotation within the estimation window. A recent method proposed by Zebker and Chen consists, for instance, in dividing the interferogram into 8×8 or 16×16 pixel windows and measuring the local dominant fringe patterns in the Fourier domain [23].

In this paper, we propose to improve these approaches and to adapt them to the new context of high-resolution (HR) interferograms. An original two-step method for estimating local frequencies is presented. The first step estimates the main fringe pattern on large boxcar windows by using existing methods. It provides a robust estimation of the average local frequency corresponding to the so-called "LR" fringe pattern. The second step consists in removing this main fringe pattern and estimating the remaining local fringe patterns due to local variations, which are missed in the first step for different reasons such as

- difference between the fringe model estimated in the first step and the real fringes;
- local aliasing when the LR fringes are already high frequency and local variations increase the fringe rate;
- discontinuities of the fringe pattern within the LR estimation boxcar window.

To estimate the local frequency corresponding to the so-called "HR" fringe pattern, we propose to use intensity-driven adaptive neighborhoods (IDANs) that are more likely to follow the local fringe variations and a new method to estimate the 2-D local frequencies on such neighborhoods with variable shape and size. The key issue when using the algorithm proposed in [10] lies in the fact that surface orientation is highly correlated with SAR intensity values. This observation is valid mainly for glacial areas, where the presence of other factors influencing the SAR intensity signal is highly reduced. Results are presented using two different data sets over the Mer-de-glace—the Leschaux and the Tacul glaciers, which are located in the Mont-Blanc area: a simulated interferogram obtained from an HR DTM computed from aerial photographs, and a real interferogram from an airborne Experimental SAR (E-SAR) campaign that took place in this area in October 2006.

The remainder of this paper is organized as follows. Section II is dedicated to the presentation of the local frequency estimation algorithm. In Section III, the results obtained using the proposed approach are presented and compared to those given by previous methods developed in the framework of ERS interferograms. Both simulated and real interferograms are used. Results of phase unwrapping and interferogram filtering are also given, starting from the obtained frequency estimates. In Section IV, some conclusions and perspectives are presented. Eventually, Appendix briefly describes the principles of the 2-D local frequency estimation technique [18] used with boxcar windows for the LR fringe pattern analysis.

II. HIGH-RESOLUTION FRINGE PATTERN ANALYSIS

Under the assumption of a large number of scatterers inside the resolution cell, the statistics of the interferometric phase

have been completely characterized [19]. Several interferogram filtering strategies have been reported [24]–[27].

Lee *et al.* proposed a spatially adaptive filtering method for improving the accuracy of the interferometric phase estimation [28]. The basic idea of the filter is to preserve edges and to better filter noise in their vicinity. A set of 16 directional subwindows are defined to locate the optimal estimation samples inside the considered neighborhood. The subwindow selection procedure is performed either after locally applying the phase unwrapping procedure or operating in the complex plane. Only the pixels in the selected subwindow are used to compute the filtered value, which is derived from the locally linear minimum mean-squared error estimator. In [12], a multiscale interferogram analysis is proposed. The phase image is locally analyzed in the Shannon wavelet domain, and the filter is characterized by good spatial resolution maintenance properties.

This paper presents a new method to obtain the local frequencies within an interferogram by fusing multiscale analysis technique [11], multivariate adaptive neighborhood (AN) estimation algorithm [10], and robust LR squared fixed-size windowing procedure [18]. This can only be achieved due to a new adaptive 2-D frequency estimator dedicated to neighborhoods with variable shape and size.

A. Proposed Model

For each pixel of the interferogram, the 2-D phase signal ϕ is considered as having two deterministic components as follows:

- the LR phase ϕ_{LR} corresponding to the average fringe pattern created by the LR features;
- the HR phase ϕ_{HR} corresponding to the local difference of the phase signal with the average fringe pattern. This component is induced by HR features.

Furthermore, one random component corresponding to the phase noise ϕ_n is added. Consequently, the analytical phase signal can be written as

$$e^{j\phi} = e^{j\phi^{\mathrm{LR}}} e^{j\phi^{\mathrm{HR}}} e^{j\phi_n}. \tag{1}$$

LR and HR components do not correspond to a partition of the frequency domain such as low or high frequencies, but to the spatial resolution of the associated fringe pattern. In the case of topographic fringes for instance, the LR phase corresponds to the mean slope of the area covered by a large estimation window [Fig. 2(a)], whereas the HR phase corresponds to smaller scale additional variations around this average slope due to the microrelief [Fig. 2(b)].

The first step of the proposed algorithm consists in estimating the LR phase and removing the associated fringe pattern. This is performed by estimating the 2-D LR local frequency with a modified version of the MUSIC algorithm [18]. The method consists in building a 1-D signal vector by appending the lines of a small rectangular sliding subwindow. Then, the covariance matrix of this vector is estimated within a larger window. The estimation of the two frequency components is based on the structure of the vector covariance matrix (VCM) described in the Appendix. The principle of this VCM method requires large
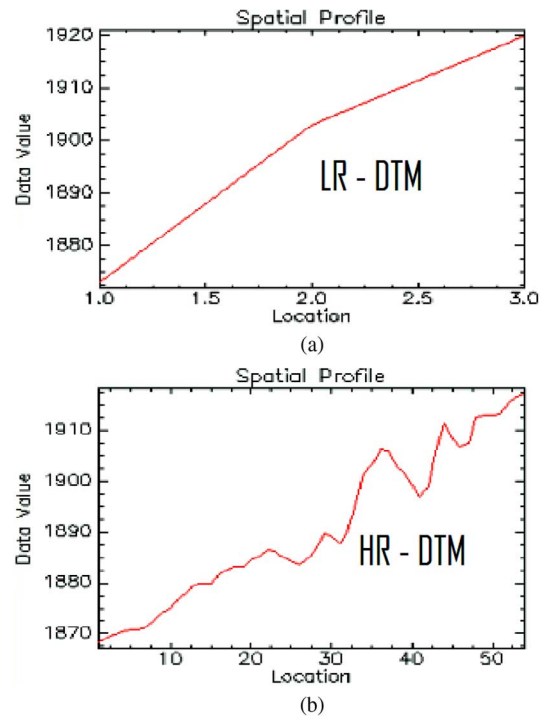

Fig. 2. DTM profile on the Mer-de-glace glacier. (a) Using DTED-1 LR DTM (Res = 80 m). (b) Using HR DTM (Res = 2 m).

rectangular estimation windows, and it cannot be applied to irregular ANs.

B. Spatial Support

In the second step, the local HR frequencies are estimated. The proposed procedure consists in gathering only the pixels that belong to the same HR spatial feature and fulfill the "local stationarity" hypothesis [29]. We assume that small homogeneous regions within the two intensity images correspond to ground areas with a homogeneous cover and a constant orientation which should respect the stationarity hypothesis. Although not generally valid for any type of terrain (particularly flat vegetation or urban areas), this assumption is verified for rather steep-sloped temperate glaciers that are encountered over 1500 m above sea level (ASL) in the Alps. As a consequence, the information that is provided by the intensity multivariate vector is suitable to build IDAN [10]. Even if these neighborhoods are not exactly "fringe pattern driven," they are more likely to respect the stationarity hypothesis than blind boxcar windows according to the following considerations.

- Within a full SAR scene, the local variation of the backscattered radar radiation strongly depends on the local surface orientation of the targeted area. In software such as ROI-PAC for instance, the knowledge of the slope orientation provided by a DTM is sufficient to simulate SAR image and to register them on real ERS or ENVISAT images. If the LR SAR data are mainly sensitive at the mean slope, the new HR SAR systems will more accurately reflect the small slope variations induced by the local microrelief.

- The local variations of the backscattered radar radiation imposed by local changes of the dielectric and magnetic permittivities may not be directly linked to phase nonstationarity. However, they are potential sources of different backscattering mechanism or temporal evolutions yielding to different coherence level in large baseline or repeat-pass interferometry. For instance, it allows discriminating between rocks and ice or different snows in the particular context of Alpine glaciers.

The main advantage of the IDAN method is to gather a significant number of samples in an estimation window where stationarity is simultaneously preserved with respect to the two intensity images.

The two master I_1 and slave I_2 intensity images are considered as a bivariate image as follows:

$$p(m, n) = [I_1(m, n), I_2(m, n)]^T. \tag{2}$$

The proposed AN determination relies on the image $p(m, n)$ and involves processing vectorial images mixed with multiplicative noise model. The algorithm consists of the following steps [10].

1) *Rough estimation of the seed value:* Compute the marginal median $\widehat{p}(m, n)$ in the 3×3 centered neighborhood.
2) *Region growing:* The eight direct neighbors $p(m', n')$ of the seed are accepted inside the AN provided they meet the following condition:

$$\frac{\|p(m', n') - \widehat{p}(m, n)\|}{\|\widehat{p}(m, n)\|} \leq T_1, \qquad T_1 = \frac{2}{3} \frac{\sigma_n}{\mu_n}. \tag{3}$$

Threshold T_1 is set according to the speckle mean μ_n and standard deviation σ_n, which are *a priori* known constants, as they both depend on the initial number of looks L and are identical for both intensity images. Then, the same procedure is applied for all of the neighbors of the newly included pixels and so on. The region growing is iterated until either the number of pixels already included in the AN exceeds a predefined upper limit $N_{\max}$ or none of the new neighbors fulfills the test condition (3). The pixels that have already been tested but not accepted inside the AN (called *background pixels* in the following) are stored in a separate list.
3) *Refined estimation of the seed value:* A more reliable estimator of the unspeckled seed value $\overline{p}(m, n)$ is now obtained by averaging the pixels included in the AN defined in the previous step.
4) *Reinspection of the background pixels:* The background pixels $p(o, r)$ of the list created in step 2) are tested again and aggregated in the AN provided that

$$\frac{\|p(o, r) - \overline{p}(m, n)\|}{\|\overline{p}(m, n)\|} \leq T_2, \qquad T_2 = 2T_1. \tag{4}$$

The AN is updated accordingly. The test is less restrictive, as the inclusion threshold is twice as large as the one used in the first step of the region growing procedure.

C. Autocorrelation Function

One major advantage of the AN lies in the fact that its shape adapts to the useful signal. This allows the shape of the spatial support to be irregular. As a consequence, conventional estimators of the local frequency, such as VCM [18] or Fourier transform [23], cannot be used with AN.

This section introduces a new adaptive 2-D frequency estimator that can be successfully applied in the specific case of ANs. The main idea is to use the previously obtained AN as spatial support for computing the 2-D autocorrelation function of the phase signal.

Using 2-D notation, the phase signal is modeled by a first-order approximation corresponding to a 2-D complex sine wave with frequency (f_x, f_y) and additive noise ϕ_n as

$$s(k, l) = e^{j\phi(k, l)} = e^{j[2\pi(kf_x + lf_y) + \phi_n]}. \tag{5}$$

The autocorrelation coefficients are defined by

$$\gamma(p, q) = E\left\{s(k, l) \cdot \overline{s(k - p, l - q)}\right\} \tag{6}$$

where $E\{\cdots\}$ denotes the mathematical expectation and $\overline{s(k - p, l - q)}$ denotes the complex conjugate of $s(k - p, l - q)$.

Under the assumption that the phase noise is an additive independent identically distributed random process, we obtain

$$\gamma(p, q) = K\, e^{j\, 2\pi(pf_x + qf_y)} \tag{7}$$

where $K = |\langle e^{j\, \phi_n(0)}\rangle|^2$ is a real coefficient that does not affect the autocorrelation phase anymore.

As the stationarity and ergodicity conditions are assured, the autocorrelation function is computed by spatial averaging of the products $s(k, l) \cdot \overline{s(k - p, l - q)}$ for all the possible delays (p, q) within the AN. One can notice that the reliability of the $\gamma(p, q)$ estimation strongly depends on the available number $N_{p,q}$ of pairs of pixels delayed with (p, q). Then, the local frequencies can be estimated from two consecutive values of the autocorrelation function (on lines or on rows). The proposed algorithm estimates the components of the 2-D frequency as the arguments of the following sums:

$$\widehat{f}_x = \frac{1}{2\pi} \cdot \arg\left[\sum_{(p,q)} N_{p,q} N_{p+1,q} \cdot \gamma(p+1, q)\overline{\gamma(p, q)}\right] \tag{8}$$

$$\widehat{f}_y = \frac{1}{2\pi} \cdot \arg\left[\sum_{(p,q)} N_{p,q} N_{p,q+1} \cdot \gamma(p, q+1)\overline{\gamma(p, q)}\right]. \tag{9}$$

By weighting the estimated value $\gamma(p, q)$ by $N_{p,q}$, the more reliable samples become more important.

Moreover, for each component $\widehat{f}_x$ and $\widehat{f}_y$, a confidence measure $\mathcal{C}_{f_x}$ (respectively $\mathcal{C}_{f_y}$) is defined by the ratio of the
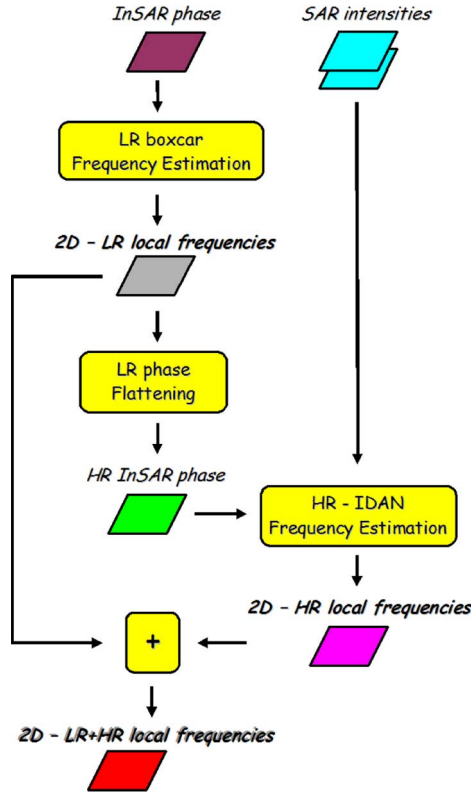
Fig. 3. Block diagram of the proposed method.

TABLE I
PROCESSING PARAMETERS FOR TerraSAR-X IMAGE SIMULATION

Parameter	Value
satellite altitude (km)	514
ground sampling (m)	2
azimuth sampling (m)	2
range sampling (m)	1.2
viewing angle at close range (degrees)	30
altitude of ambiguity (m)	10
coefficient of variation	0.52
uniform phase noise distribution	$\pm\pi/4$

The resulting HR phase signal $e^{\phi_{fl}}$ exhibits the local differences between the 2-D sine-wave model and the real fringe pattern. Second, the 2-D HR frequency $(f_x^{\mathrm{HR}}, f_y^{\mathrm{HR}})$ of the HR phase signal is estimated from the 2-D autocorrelation function using IDANs as spatial support.

According to the Nyquist–Shannon criterion, when the local variation $\Delta\phi$ of the phase signal belongs to the $[-\pi, \pi]$ interval, its local frequency f belongs to $[-0.5, 0.5]$. The proposed two-step method first estimates the 2-D LR spatial frequency $(f_x^{\mathrm{LR}}, f_y^{\mathrm{LR}})$ in the domain $[-0.5, 0.5] \times [-0.5, 0.5]$. After the removal of this average fringe pattern, the 2-D HR frequency $(f_x^{\mathrm{HR}}, f_y^{\mathrm{HR}})$ can also be estimated in the domain $[-0.5, 0.5] \times [-0.5, 0.5]$. In the case of local aliasing due to HR features, which makes the magnitude of a frequency component higher than 0.5 and lower than 1, the LR + HR model is able to recover this component and yields a total of 2-D frequency $(f_x^{\mathrm{LR}} + f_x^{\mathrm{HR}}, f_y^{\mathrm{LR}} + f_y^{\mathrm{HR}})$, which belongs to the domain $[-1, 1] \times [-1, 1]$. In other words, the proposed method is also able to retrieve phase gradients in limited aliased areas where $\Delta\phi$ belongs to $[-2\pi, 2\pi]$.

Finally, the obtained local frequencies can be directly used as input for either SAR data filtering [9] or phase unwrapping [20].

magnitude of the complex sum over the sum of the magnitudes as

$$\mathcal{C}_{f_x} = \frac{\left| \sum_{(p,q)} N_{p,q} N_{p+1,q} \cdot \gamma(p+1,q)\overline{\gamma(p,q)} \right|}{\sum_{(p,q)} N_{p,q} N_{p+1,q} \cdot \left| \gamma(p+1,q)\overline{\gamma(p,q)} \right|}. \quad (10)$$

When all the different products $\gamma(p+1,q)\overline{\gamma(p,q)}$ have the same argument, the confidence is equal to 1 and reveals a good agreement between the fringe pattern and the complex sine-wave model. On the contrary, the confidence decreases when the products $\gamma(p+1,q)\overline{\gamma(p,q)}$ have different arguments, due to unreliable estimation of the autocorrelation function or disagreement with the model. The global confidence $\mathcal{C}_f = \min(\mathcal{C}_{f_x}, \mathcal{C}_{f_y})$ is taken as the minimum of the two confidences to reveal an unreliable 2-D frequency estimate as soon as one of the two components is not reliable.

III. RESULTS AND DISCUSSION

The proposed method has been tested on the "Chamonix-Mont-Blanc" test site which is located in the Alps, near the borders between France, Italy, and Switzerland (45°50′ N, 6°51′ E). It includes the Aiguille-Verte (4122 m ASL), the Chamonix valley (1000 m ASL), and several instrumented glaciers. The results presented in this section have been obtained on simulated TerraSAR-X HR data and on airborne E-SAR data over a group of three glaciers: 1) the well-known Mer-de-glace glacier and in its upper part; 2) the Leschaux glacier; and 3) the Tacul glacier.

D. Application to SAR Interferograms

The block diagram of the proposed two-step algorithm for local frequency estimation is presented in Fig. 3. First, an LR phase flattening is performed by using the 2-D LR frequency $(f_x^{\mathrm{LR}}, f_y^{\mathrm{LR}})$ estimated by the VCM method [18]. In each pixel (m,n) of the interferogram, the global fringe pattern is approximately removed in the surrounding pixels (k,l) by computing the following flattened phase ϕ_{fl}:

$$\phi_{fl}(k,l) = \phi(k,l) - 2\pi \left[(k-m)f_x^{\mathrm{LR}} + (l-n)f_y^{\mathrm{LR}} \right]. \quad (11)$$

A. Simulated TerraSAR-X InSAR Data

To illustrate the proposed method on HR data over Alpine glaciers, a 2-m resolution DTM of the Mer-de-glace [15] has been used to simulate the SAR amplitude of TerraSAR-X images using the method proposed in [30]. The parameters used in the simulation are presented in Table I.

Fig. 4(a) and (b) presents a real ERS amplitude (∼20-m resolution) and the simulated TerraSAR-X amplitude (∼2-m resolution), respectively. The area corresponds to a part of the
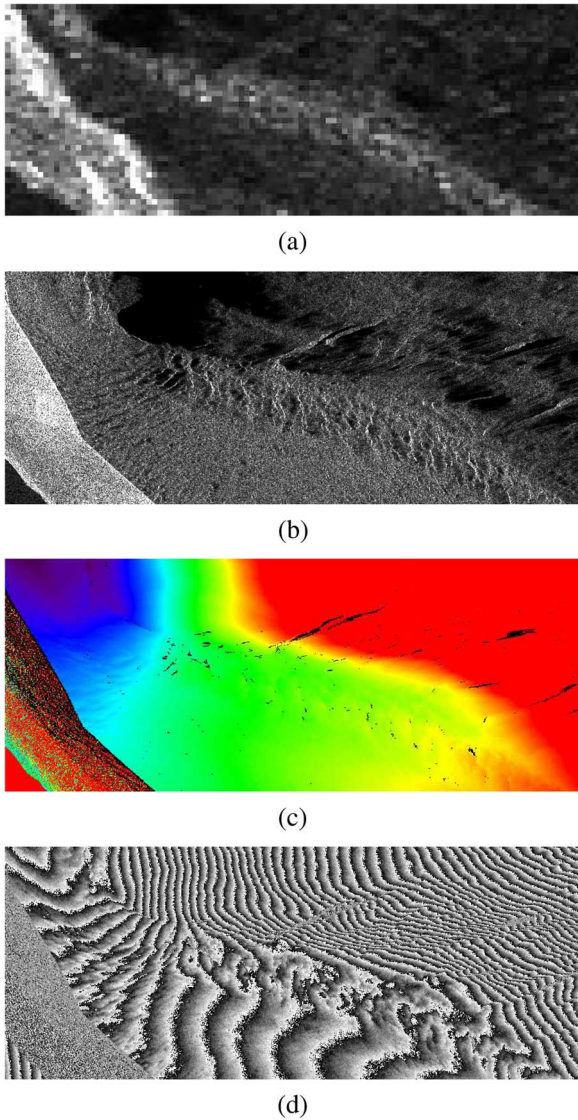
(a)

(b)

(c)

(d)

Fig. 4.   Mer-de-glace glacier (840 × 340 pixels). (a) ERS-1 five-look amplitude. (b) Simulated one-look TerraSAR-X amplitude. (c) Elevation image in TerraSAR-X slant range geometry. (d) Simulated one-look TerraSAR-X phase.
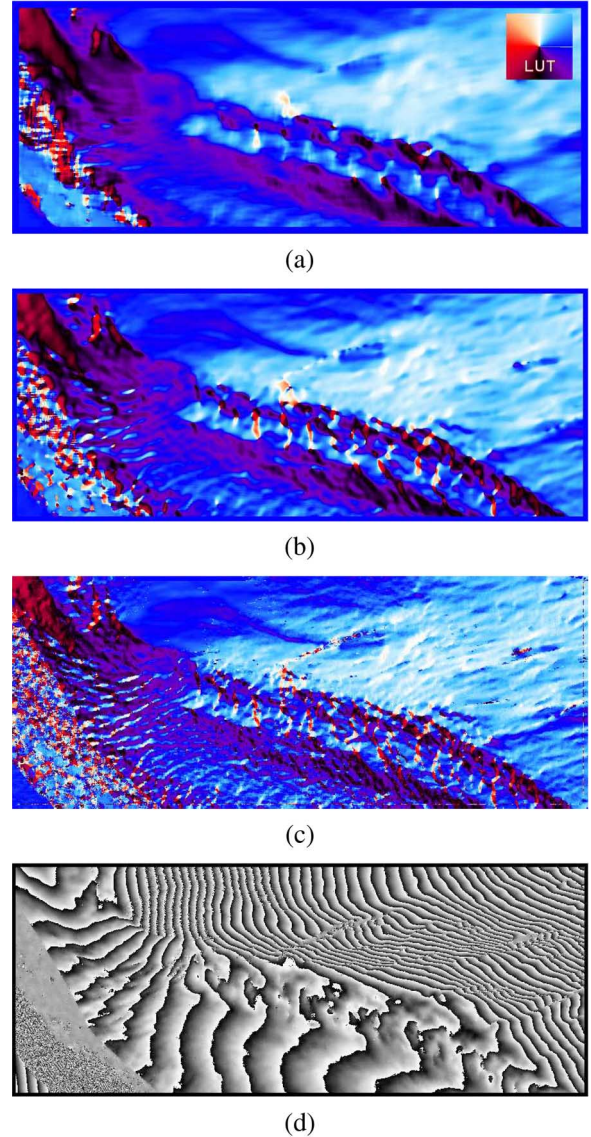

(a)

(b)

(c)

(d)

Fig. 6.   Orientation map of the local fringe pattern with TerraSAR-X (840 × 340 pixels). (a) LR with VCM 11 × 11 (local fringe orientation lookup table in the right upper corner). (b) VCM 7 × 7. (c) Sum of the LR and the HR components. (d) IDAN filtered phase with LR + HR phase flattening.
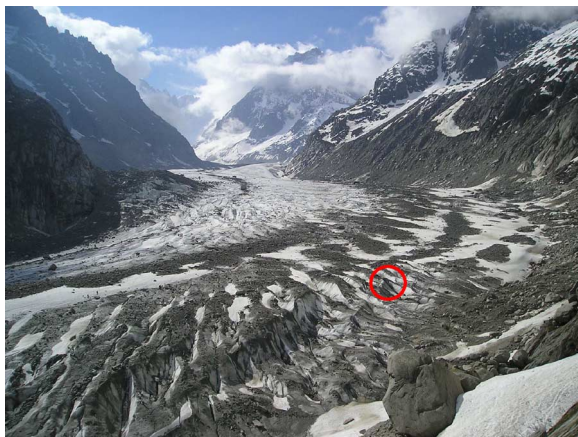

Fig. 5.   May 2004: Photo of the simulated TerraSAR-X region on the Mer-de-glace glacier (approximate position of the profile in Fig. 7 marked in red).

Mer-de-glace glacier illustrated in Fig. 5. The altitude information provided by the DTM has been resampled in a TerraSAR-X slant range geometry [Fig. 4(c)] and converted into topographic fringes modulo a tunable altitude of ambiguity [Fig. 4(d)]. A controlled noise level was also introduced on the resulting HR phase and amplitude images. The comparison with LR image, such as the ERS acquisition illustrated in Fig. 4(a), shows that small relief variations become visible in the HR images, and the presence of crevasses can be noticed.

Fig. 6 illustrates the fringe orientation maps computed from the frequency estimates over the Mer-de-glace glacier and the Les-Echelets flank. A colored lookup table, which is provided in Fig. 6(a), is used to indicate the main slope orientation derived from the fringe pattern 2-D local frequency. Most of the local topographic information is missed by the LR frequency estimation illustrated in Fig. 6(a). It can be observed in Fig. 6 that the LR + HR local frequency estimates provide

TABLE II
RMSE OF THE 2-D LOCAL FREQUENCY (f_x, f_y) ESTIMATED BY A
SINGLE-RESOLUTION APPROACH (BOXCAR 7×7) AND THE PROPOSED
MULTIRESOLUTION LR + HR APPROACH (LR FREQUENCY: BOXCAR
11×11, HR FREQUENCY: 50-SAMPLE IDAN). REFERENCE: ELEVATION
GRADIENT COMPUTED IN THE TerraSAR-X SLANT RANGE GEOMETRY

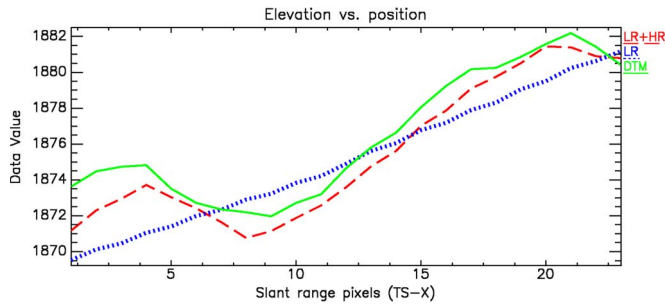|	RMSE f_x	RMSE f_y
VCM 7x7	3.6105e-004	3.5952e-004
LR+HR	**1.8823e-004**	**1.9998e-004**

Fig. 7. Spatial profile (50 m) along the surface of the Mer-de-glace glacier. (In green) Real altitude resampled in the TerraSAR-X slant range. (In red) Unwrapped HR + LR estimates of the local frequencies. (In blue) Unwrapped LR estimates of the local frequencies.

a more robust mapping of the local topography variations due to crevasses (see red mark in Fig. 5). Fig. 6(d) shows the IDAN filtered interferogram obtained by taking the estimated deterministic fringe pattern presented in Fig. 6(c) into account. The result is in accordance with the local topography variations observed in the original radar-coded altitude information [Fig. 4(c)].

The use of simulated HR interferogram allows objective performance assessments. A comparison between a conventional frequency estimation on a boxcar window and the multiresolution LR + HR proposed method has been performed by measuring the accuracy of the 2-D frequency estimates. The root-mean-square error (RMSE) has been computed using, as reference, the phase gradient measured by Prewitt kernels in the SAR-coded elevation map [Fig. 4(c)]. The results reported in Table II have been obtained by

- single-resolution approach using the VCM method on conventional boxcar windows with a 7×7 size which is a good compromise between robust estimation and spatial resolution preservation;
- LR + HR frequency estimation, LR by VCM method on large boxcar sliding window (11×11) and HR by the new algorithm on AN (50 samples).

The RMSE of the proposed method is significantly lower (almost divided by 2) than the RMSE of conventional boxcar estimation.

The importance of the HR frequency component can be assessed by directly injecting the 2-D local frequencies in least-squares phase unwrapping [20], [22]. The simulated interferogram has been unwrapped from the LR local frequency estimates and from the LR + HR estimates. After multiplying with the corresponding altitude of ambiguity and zero origin

TABLE III
AIRBORNE SAR DATA ACQUIRED OVER THE TEST AREA

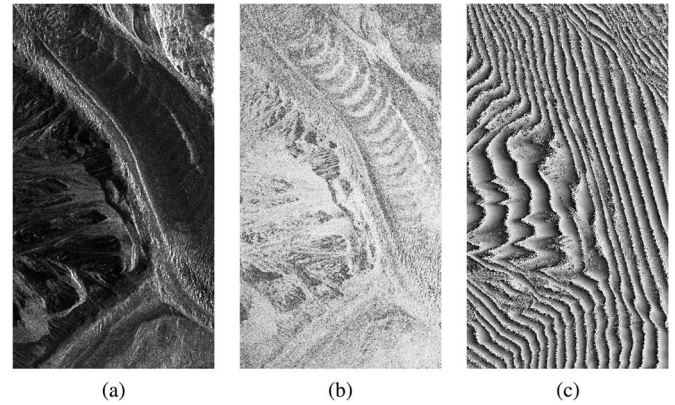| Agency	DLR-HR
campaign	MEGATOR
date	06.10.10
sensor	E-SAR
test site	Chamonix Mont-Blanc
band	L
polarization	HH
SLC range sampling (m)	1.5
SLC azimuth sampling (m)	0.45
altitude above MSL (m)	6040.48
Δt (min)	16.4
$B_{\parallel}$ (m)	0.12
$B_{\perp}(m)$	-9.79

Fig. 8. E-SAR (16-look) interferogram (392×709 pixels). (a) Master amplitude. (b) Coherence map. (c) Interferometric phase.

correction, the two results can be compared to the real altitude available from the HR DTM, which are resampled in the TerraSAR-X slant range. Fig. 7 presents a 50-m spatial profile along the surface of the Mer-de-glace glacier. The approximate position of the profile is marked in red in Fig. 5. Although the VCM LR unwrapped phase is rather linear, the proposed method follows the fractal shape induced by the local altitude variation.

B. Airborne InSAR Data

The proposed method has been applied on real HR InSAR data acquired by the E-SAR airborne system over the upper part of the Mer-de-glace glacier (the Tacul and Leschaux glaciers). A campaign with SAR image acquisitions and *in situ* measurements has been organized in October 2006, in collaboration between the German Aerospace Center (DLR) and the French laboratories of the MEGATOR project [15]. The parameters of the data set used to illustrate the performances of the proposed method are reported in Table III.

The amplitude, coherence, and phase images of a 10-m baseline L-band interferogram are illustrated in Fig. 8. On the amplitude and the coherence images, one can observe the curved stripes that correspond to the Forbes band phenomena. This periodical feature indicates the one-year displacement of the Tacul glacier, and it is explained by the fact that during the
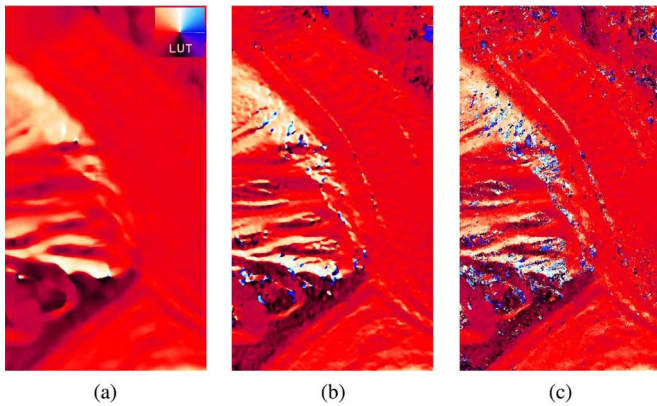
(a)   (b)   (c)

Fig. 9. Orientation map of the local fringe pattern with E-SAR (392 × 709 pixels). (a) LR with VCM 11 × 11 (local fringe orientation lookup table in the right upper corner). (b) VCM 7 × 7. (c) Sum of the LR and the HR components.

(a)   (b)   (c)

Fig. 10. E-SAR L-band SAR data (392 × 709 pixels). (a) Boxcar 7 × 7 filtered coherence with VCM 7 × 7 phase flattening. (b) IDAN filtered coherence with LR + HR phase flattening. (c) Confidence map for HR frequency estimation.

summer season, a large amount of rocks fall on the ice in the upper part of the glacier and almost none in winter when rocks are much more stable. This phenomenon produces the smooth "staircase" shape in the upper part of the Tacul glacier. On the interferogram [Fig. 8(c)], the fringe pattern has two main components: 1) the topography and 2) the range evolution of the path difference (the so-called orbital fringes in the case of spaceborne data).

The results of the 2-D local frequency estimation performed at LR and the final combined LR and HR estimates are illustrated in Fig. 9 by the orientation of the corresponding phase gradient. For comparison, the orientation of the local fringe pattern computed using VCM on nonadaptive 7 × 7 squared centered neighborhood is presented in Fig. 9(b). As expected, the LR result in Fig. 9(a) is smooth and robust but it does not follow the local variations of the fringe pattern neither along the glacier surface nor on the surrounding mountains. This missing information is present in the sum of the LR and the HR components, which provides a more robust and more precise estimate of the local fringe pattern. One can notice a clear resolution improvement over the Forbes bands, where the local small slope variation is completely lost in the LR estimate and is hardly visible in the 7 × 7 VCM estimate. The local slope orientation along the Western side of the Aiguille-du-Tacul mountain (left side of Fig. 9) is more accurately estimated with the proposed algorithm.

Fig. 10(b) presents the coherence filtering results obtained with the IDAN filter [9], using the deterministic fringe pattern compensation provided by the HR and LR local frequency estimation [Fig. 9(c)]. The confidence image in Fig. 10(c) was thresholded to avoid using unreliable estimation of the HR fringe pattern. The value empirically chosen for the threshold is 0.4. In addition, the coherence map filtered with the 7 × 7 boxcar filter and the VCM 7 × 7 estimated local frequencies [Fig. 9(b)] are illustrated in Fig. 10(a).

Several different factors influence the coherence estimation, such as the true coherence value itself, the number of sample averaged to reduce estimation bias and variance, and the respect of the local stationarity assumption. To investigate the influence of the frequency estimates and the use of ANs on coherence
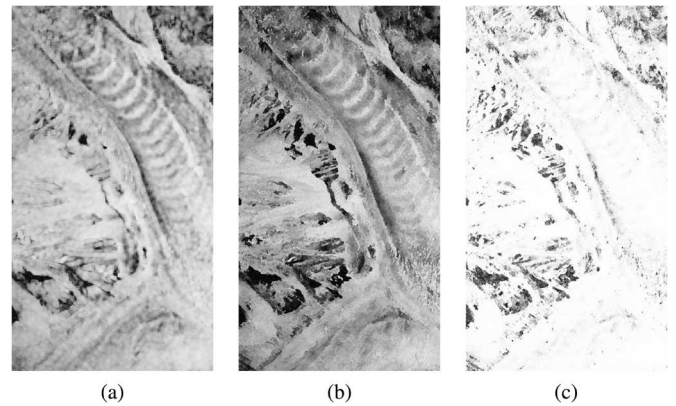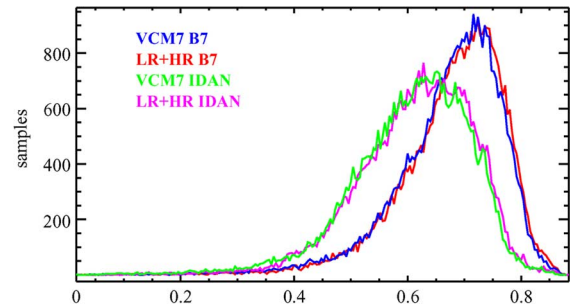

Fig. 11. Histograms of filtered coherence maps over the Tacul glacier. (In red) Boxcar 7 × 7 with LR + HR phase compensation. (In blue) Boxcar 7 × 7 with 7 × 7 VCM phase compensation. (In magenta) IDAN with LR + HR phase compensation. (In green) IDAN with 7 × 7 VCM phase compensation.

maps, four coherence histograms have been computed in the following cases:

- by flattening with the 7 × 7 VCM (VCM7) and estimating coherence on boxcar (B7) or adaptive neighborhoods (IDANs);
- by flattening with LR plus HR frequency (LR + HR) and estimating the coherence on B7 sliding window or on IDAN.

Histograms in Fig. 11 show the results obtained on the E-SAR interferogram. The use of the AN instead of the boxcar for complex multilooking has a stronger effect on the coherence level than the use of an adaptive multiresolution frequency estimation technique instead of a nonadaptive one. In this particular case, the bulk of the improvement can be achieved by phase slope compensation with boxcar frequency estimation; hence, the coherence levels are affected only in small areas with local strong variations of the fringe pattern. However, it can be noticed that in both cases (boxcar and IDAN), the LR + HR frequencies have slightly improved the results compared to the VCM frequencies. The lower coherence obtained with the ANs is due to the larger number of samples averaged by IDAN with a stop criterion $N_{max} = 100$ compared to the 49 samples averaged by the 7 × 7 boxcar. Lower coherence can be interpreted as a benefit of the proposed method (a reduction of the coherence overestimation due to a sufficient averaging)

or by a drawback if the lower values are due to the averaging of heterogeneous pixels in nonstationary areas. According to the previous results, regarding IDAN coherence estimation [10] and the visual improvement of the filtered coherence and phase images, it seems reasonable to interpret the coherence decrease by the "positive" explanation rather than by a lack of stationarity over the AN.

In conclusion, the different factors that affect the coherence and the lack of "ground truth" make it difficult to illustrate an improvement of the frequency estimation through the coherence level histograms. The main benefit of the proposed method, regarding coherence estimation, is the use of the same AN for both frequency estimation and coherence filtering to preserve the HR of the data.

IV. CONCLUSION AND PERSPECTIVES

The increased performances of future HR SAR systems (TerraSAR-X, COSMO-SKYMED, or Radarsat-2) together with the developments of appropriate processing algorithms reinforce the potential of SAR interferometry for temperate glacier periodic monitoring. A new method has been proposed to estimate the local frequencies within HR interferograms by a multiresolution algorithm: LR 2-D frequency are estimated on large boxcar windows by previous estimation methods such as VCM [18] and HR 2-D fringe pattern remaining after LR phase flattening are analyzed by measuring their local frequency on IDANs. This method is adapted to deal with the small ground resolution cells and small altitudes of ambiguity, which makes the fringe pattern sensitive to the local topographic variations.

In the context of temperate glacier activity monitoring, it can be applied to improve the processing of HR interferograms to derive, for instance, very accurate DTM and differential DTM to obtain volume balances. In this case, HR frequency estimation combined with intensity-driven neighborhood techniques provides very good results since most of the sources of phase nonstationarity are revealed by the SAR intensities, which are mostly influenced by the local slope. It will also be useful for differential interferometry to obtain HR velocity field measurements that require efficient phase filtering and unwrapping methods. In this case, one difficulty that has to be addressed in future works is the presence of phase nonstationarity that is more related to the glacier displacement models and independent from the amplitude information. Future work should also investigate different strategies to perform HR fringe pattern analysis in different contexts, where the intensity information would not be dominated by the topography (urban areas, agricultural regions, etc.). A fusion of different information sources such as the coherence or the phase gradient would make the method applicable in more general terrain.

APPENDIX

The VCM method [18] used to estimate the 2-D local frequencies (f_x, f_y) of SAR interferograms on boxcar windows is based on the structure of a "signal vector" resulting from the concatenation of the lines of a 2-D complex sine-wave signal $s(m, n) = e^{i\phi(m,n)} = e^{i2\pi(m \cdot f_x + n \cdot f_y)}$. If this signal is observed on a $N_s \times N_s$ subwindow (square for the sake of simplicity), the size of the "signal vector" $\underline{v_s}$ is N_s^2 and the size of its covariance matrix Γ_s is $N_s^2 \times N_s^2$. With this model, Γ_s can be written as

$$\Gamma_s = \underline{v_s} \cdot \underline{v_s}^\dagger = \begin{bmatrix} 1 \\ e^{j\,2\pi \cdot f_x} \\ e^{j\,2\pi \cdot 2f_x} \\ \cdots \\ e^{j\,2\pi(N_s-1)f_x} \\ --- \\ e^{j\,2\pi \cdot f_y} \\ e^{j\,2\pi \cdot (f_x+f_y)} \\ \cdots \\ e^{j\,2\pi((N_s-1)f_x+f_y)} \\ --- \\ \cdots \end{bmatrix} \begin{bmatrix} \underline{v_s}^\dagger \end{bmatrix}.$$

Accordingly, this covariance matrix presents a $N_s \times N_s$ block structure: inside the blocks, lines are equal to the previous lines multiplied by $a_x = e^{i2\pi \cdot f_x}$ and each block is equal to the previous block multiplied by $a_y = e^{i2\pi \cdot f_y}$. This block structure can be used to estimate the 2-D local frequencies of SAR interferograms by the following three-step algorithm:

1) estimate the $N_s^2 \times N_s^2$ VCM under the stationarity and ergodicity hypothesis by complex averaging on a $N_e \times N_e$ sliding window, with $N_e > N_s$ to average $(N_e - N_s + 1)^2$ matrix samples;
2) compute by least-squares estimation the coefficients a_x and a_y;
3) derive the frequency estimates $\hat{f}_x$ and $\hat{f}_y$ from the arguments of these coefficients.

ACKNOWLEDGMENT

REFERENCES

[1] A. Fischer, H. Rott, and H. Björnsson, "Observation of recent surges of Vatnajökull, Iceland, by means of ERS SAR interferometry," *Ann. Glaciol.*, vol. 37, no. 69, pp. 69–76, 2003.
[2] K. E. Mattar, P. W. Vachon, D. Geudtner, A. L. Gray, I. G. Cumming, and M. Brugman, "Validation of alpine glacier velocity measurements using ERS tandem-mission SAR data," *IEEE Trans. Geosci. Remote Sens.*, vol. 36, no. 3, pp. 974–984, May 1998.
[3] D. Massonnet, F. Adragna, and M. Rossi, "CNES general-purpose SAR correlator," *IEEE Trans. Geosci. Remote Sens.*, vol. 32, no. 3, pp. 636–643, May 1994.
[4] P. A. Rosen, S. Hensley, I. R. Joughin, F. K. Li, S. N. Madsen, E. Rodriguez, and R. M. Goldstein, "Synthetic aperture radar interferometry," *Proc. IEEE*, vol. 88, no. 3, pp. 333–382, Mar. 2000.
[5] P. A. Rosen, S. Hensley, G. Peltzer, and M. Simons, "Updated repeat orbit interferometry package released," *EOS, Trans. Amer. Geophys. Union, Electron. Suppl.*, vol. 85, no. 5, p. 47, 2004.
[6] T. Strozzi, A. Luckman, T. Murray, U. Wegmuller, and C. L. Werner, "Glacier motion estimation using SAR offset-tracking procedures," *IEEE Trans. Geosci. Remote Sens.*, vol. 40, no. 11, pp. 2384–2391, Nov. 2002.
[7] A. L. Gray, N. Short, K. E. Matter, and K. C. Jezek, "Velocities and ice flux of the Filchner ice shelf and its tributaries determined from speckle tracking interferometry," *Can. J. Remote Sens.*, vol. 27, no. 3, pp. 193–206, 2001.

[8] R. de Lange, A. Luckman, and T. Murray, "Improvement of satellite radar feature tracking for ice velocity derivation by spatial frequency filtering," *IEEE Trans. Geosci. Remote Sens.*, vol. 45, no. 7, pp. 2309–2318, Jul. 2007.

[9] G. Vasile, E. Trouvé, M. Ciuc, and V. Buzuloiu, "General adaptive neighborhood technique for improving SAR interferometric coherence and phase estimation," *J. Opt. Soc. Amer. A, Opt. Image Sci.*, vol. 21, no. 8, pp. 1455–1464, 2004.

[10] G. Vasile, E. Trouvé, J.-S. Lee, and V. Buzuloiu, "Intensity-driven-adaptive-neighborhood technique for polarimetric and interferometric SAR parameters estimation," *IEEE Trans. Geosci. Remote Sens.*, vol. 44, no. 6, pp. 1609–1621, Jun. 2006.

[11] G. W. Davidson and R. Bamler, "Multiresolution phase unwrapping for SAR interferometry," *IEEE Trans. Geosci. Remote Sens.*, vol. 37, no. 1, pp. 163–174, Jan. 1999.

[12] C. Lopez-Martinez and X. Fabregas, "Modeling and reduction of SAR interferometric phase noise in the wavelet domain," *IEEE Trans. Geosci. Remote Sens.*, vol. 40, no. 12, pp. 2553–2566, Dec. 2002.

[13] A. B. Surazakov and V. B. Aizen, "Estimating volume change of mountain glaciers using SRTM and map-based topographic data," *IEEE Trans. Geosci. Remote Sens.*, vol. 44, no. 10, pp. 2991–2995, Oct. 2006.

[14] R. R. Forster, K. C. Jezek, L. Koenig, and E. Deeb, "Measurement of glacier geophysical properties from InSAR wrapped phase," *IEEE Trans. Geosci. Remote Sens.*, vol. 41, no. 11, pp. 2595–2604, Nov. 2003.

[15] E. Trouvé, G. Vasile, M. Gay, L. Bombrun, P. Grussenmeyer, T. Landes, J. M. Nicolas, P. Bolon, I. Petillot, A. Julea, L. Valet, J. Chanussot, and M. Koehl, "Combining airborne photographs and spaceborne SAR data to monitor temperate glaciers: Potentials and limits," *IEEE Trans. Geosci. Remote Sens.*, vol. 45, no. 4, pp. 905–924, Apr. 2007.

[16] J. Dall, "InSAR elevation bias caused by penetration into uniform volumes," *IEEE Trans. Geosci. Remote Sens.*, vol. 45, no. 7, pp. 2319–2324, Jul. 2007.

[17] D. Massonnet and K. Feigl, "Radar interferometry and its application to changes in the Earth's surface," *Rev. Geophys.*, vol. 36, no. 4, pp. 441–500, 1998.

[18] E. Trouvé, H. Caramma, and H. Maitre, "Fringe detection in noisy complex interferograms," *Appl. Opt.*, vol. 35, no. 20, pp. 3799–3806, 1996.

[19] J.-S. Lee, K. W. Hoppel, S. A. Mango, and A. R. Miller, "Intensity and phase statistics of multilook polarimetric and interferometric SAR imagery," *IEEE Trans. Geosci. Remote Sens.*, vol. 32, no. 5, pp. 1017–1028, Sep. 1994.

[20] D. C. Ghiglia and L. A. Romero, "Robust two-dimensional weighted and unweighted phase unwrapping that uses fast transforms and iterative methods," *J. Opt. Soc. Amer. A, Opt. Image Sci.*, vol. 11, no. 1, pp. 107–117, 1994.

[21] U. Spagnolini, "2-D phase unwrapping and instantaneous frequency estimation," *IEEE Trans. Geosci. Remote Sens.*, vol. 33, no. 3, pp. 579–589, May 1995.

[22] E. Trouvé, J. M. Nicolas, and H. Maitre, "Improving phase unwrapping techniques by the use of local frequency estimates," *IEEE Trans. Geosci. Remote Sens.*, vol. 36, no. 6, pp. 1963–1972, Nov. 1998.

[23] H. A. Zebker and K. Chen, "Accurate estimation of correlation in InSAR observations," *IEEE Geosci. Remote Sens. Lett.*, vol. 2, no. 2, pp. 124–127, Apr. 2005.

[24] A. Monti Guarnieri and C. Prati, "SAR interferometry: A 'quick and dirty' coherence estimator for data browsing," *IEEE Trans. Geosci. Remote Sens.*, vol. 35, no. 3, pp. 660–669, May 1997.

[25] A. B. Suksmono and A. Hirose, "Adaptive noise reduction of InSAR images based on a complex-valued MRF model and its application to phase unwrapping problem," *IEEE Trans. Geosci. Remote Sens.*, vol. 40, no. 3, pp. 699–709, Mar. 2002.

[26] I. Baran, M. P. Stewart, B. M. Kampes, Z. Perski, and P. Lilly, "A modification to the Goldstein radar interferogram filter," *IEEE Trans. Geosci. Remote Sens.*, vol. 41, no. 9, pp. 2114–2118, Sep. 2003.

[27] N. Wu, D. F. Feng, and J. Li, "A locally adaptive filter of interferometric phase images," *IEEE Geosci. Remote Sens. Lett.*, vol. 3, no. 1, pp. 73–77, Jan. 2006.

[28] J.-S. Lee, K. P. Papathanassiou, T. L. Ainsworth, M. R. Grunes, and A. Reigber, "A new technique for noise filtering of SAR interferometric phase images," *IEEE Trans. Geosci. Remote Sens.*, vol. 36, no. 5, pp. 1456–1465, Sep. 1998.

[29] R. Touzi, "A review of speckle filtering in the context of estimation theory," *IEEE Trans. Geosci. Remote Sens.*, vol. 40, no. 11, pp. 2392–2404, Nov. 2002.

[30] A. Julea, G. Vasile, I. Petillot, E. Trouvé, J. M. Nicolas, M. Gay, and P. Bolon, "Simulation of SAR images and radar coding of georeferenced information for temperate glacier monitoring," in *Proc. OPTIM*, Brasov, Romania, May 2006, vol. 4, pp. 175–180.

Gabriel Vasile (S'06–M'07) received the B.Eng. degree in electrical engineering and computer science and the M.S. degree in image, shapes, and artificial intelligence from the University Politehnica of Bucharest, Bucharest, Romania, in 2003 and 2004, respectively, and the Ph.D. degree in signal and image processing from the Université de Savoie, Annecy-le-vieux Cedex, France.

From 2001 to 2003, he was an Engineering Assistant with the Center of Microsystems and Microstructures for Environmental Monitoring and Biomedical Applications, National Institute for Research and Development in Micro and Nanotechnologies (IMT), Bucharest. From 2006 to 2007, he was a Development Engineer with the Laboratoire Grenoble Images Parole Signal Automatique, Centre National de la Recherche Scientifique, Institut National Polytechnique de Grenoble, France. Since 2007, he has held a Centre National d'Etudes Spatiales (French Space Agency) postdoctoral fellowship and works in the French Aerospace Laboratory (ONERA), Palaiseau, France. His research interests include signal and image processing, SAR remote sensing, polarimetry, interferometry, and glacier monitoring.

Emmanuel Trouvé (M'99) received the B.Eng. degree in electrical engineering from the Ecole Nationale Superieure de Techniques Avancées, Paris, France, in 1990, the Ph.D. degree in signal and image processing from the Ecole Nationale Supérieure des Télécommunications, Paris, in 1996, and the "Habilitation à Diriger des Recherches" degree from the Université de Savoie, Annecy-le-vieux, France, in 2006.

From 1996 to 1998, he was with Thomson Marconi Sonar in Underwater Acoustic and Signal Processing. Since September 1998, he has been an Associate Professor of signal processing and computer vision with the Université de Savoie, Polytech'Savoie, and works in the Laboratoire d'Informatique, Systèmes, Traitement de l'Information et de la Connaissance (LISTIC). He was the Coordinator of the French multilaboratory MEGATOR project (Monitoring the Evolution of Alpine Glaciers by Optical and Radar Remote Sensing, 2004–2007). His research interests include SAR image processing and data fusion in remote sensing.

Dr. Trouvé is a member of the IEEE Geoscience and Remote Sensing Society Data Fusion Technical Committee.

Ivan Petillot received the B.Eng. degree in electrical engineering and computer sciences and the M.S. degree in image, information, and hypermedia from the Institut de Recherche en Informatique de Toulouse (IRIT), Toulouse, France, in 2005. He is currently working toward the Ph.D. degree at the Université de Savoie, Annecy-le-vieux, France. His dissertation is on information fusion systems for remote sensing, in the framework of the MEGATOR project.

He is with the Laboratoire d'Informatique, Systèmes, Traitement de l'Information et de la Connaissance, Université de Savoie, Polytech'Savoie, Annecy-le-vieux. His research interests include information fusion, risk assessment, and glacier monitoring.

Philippe Bolon (M'94) was born in 1956. He received the B.Eng. degree in electrical engineering and the Ph.D. degree in signal processing from the National Polytechnic Institute of Grenoble (INPG), Grenoble, France, in 1978 and 1981, respectively.

From 1984 to 1994, he was an Associate Professor with the Université de Savoie, Annecy-le-vieux, France. Since September 1994, he has been a Professor with the Université de Savoie, Polytech'Savoie, and since 2002, he has been the Head of the Laboratoire d'Informatique, Systèmes, Traitement de l'Information et de la Connaissance (LISTIC). Since 1996, he has been a member of the steering committee of the French national research group in Signal and Image Processing (GdR ISIS). His current research interests include information fusion, nonlinear image processing, image segmentation, and image analysis.

Dr. Bolon is a member of the European Association for Signal Processing (EURASIP). He was the Chairman or Cochairman of the scientific committee of the International Conference on Quality Control by Artificial Vision (QCAV) in 1997, 1998, 1999, 2001, and 2003.

Jocelyn Chanussot (M'04–SM'04) received the degree in electrical engineering from the Grenoble Institute of Technology (INP Grenoble), Grenoble, France, in 1995 and the Ph.D. degree from the Université de Savoie, Annecy-le-vieux, France, in 1998.

He was with the Automatics and Industrial Micro-Computer Science Laboratory (LAMII). In 1999, he was with the Geography Imagery Perception laboratory (GIP) for the Délégation Générale de l'Armement (DGA-French National Defense Department). Since 1999, he has been with the Laboratoire Grenoble Images Parole Signal Automatique, CNRS, Institut National Polytechnique de Grenoble, Saint-Martin-d'Hères, France, as an Assistant Professor (1999–2005), an Associate Professor (2005–2007), and a Professor (2007) of signal and image processing. He is conducting his research at the Grenoble Images Speech Signals and Automatics Laboratory (GIPSA-Lab). His research interests include statistical modeling, classification, image processing, nonlinear filtering, and data fusion in remote sensing.

Dr. Chanussot has been an Associate Editor for the IEEE GEOSCIENCE AND REMOTE SENSING LETTERS (2005–2007). He is currently an Associate Editor for the IEEE TRANSACTIONS ON GEOSCIENCE AND REMOTE SENSING and for the journal *Pattern Recognition* (2006–2008). He is the Cochair of the GRS Data Fusion Technical Committee (2005–2007) and a member of the Machine Learning for Signal Processing Technical Committee of the IEEE Signal Processing Society (2006–2008). He is the Founding President of the IEEE Geoscience and Remote Sensing French Chapter (2007).
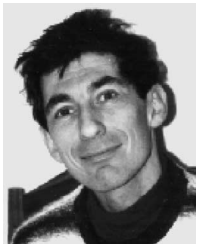
Jean-Marie Nicolas received the M.S. degree from the Ecole Normale Superieure de Saint Cloud, France, in 1979 and the Ph.D. degree in physics from the University of Paris XI, Paris, France, in 1982.

He was a Research Scientist with the Laboratoire d'Electronique Philips in medical imaging and was then with Thomson CSF, working in signal and image processing. He is currently a Professor with the Département Traitement du Signal et des Images, CNRS, Ecole Nationale Supérieure des Télécommunications, Paris, France. His current research interests include radar imaging.

Tania Landes received the B.Eng. degree in geodetic surveying and topography from the Institut National des Sciences Appliquées (INSA) de Strasbourg, Strasbourg Cedex, France, in 1995 and the Ph.D. degree in radar remote sensing from the University of Karlsruhe, Karlsruhe, Germany.

Since 2006, she has been an Associate Professor with the Equipe Photogrammétrie et Géomatique, CNRS, INSA de Strasbourg. She belongs to the "Photogrammetry and Geomatics Group" of the UMR MAP 694 research center. Her current research interests include remote sensing and laser grammetry.

Michel Gay received the B.Eng. degree in electrical engineering from the Institut des Sciences de l'Ingénieur de Montpellier, Montpellier, France, in 1987 and the Ph.D. degree in physics from the University Joseph Fourier, Grenoble, France, in 1999.

From 1988 to 2003, he was with Cemagref Grenoble, Grenoble, in electrical engineering for environmental applications. Since 2003, he has been a Research Engineer with the Laboratoire Grenoble Images Parole Signal Automatique, CNRS, Institut National Polytechnique de Grenoble, Saint-Martin-d'Hères, France. His research interests include remote sensing, image processing, and survey of Alpine glaciers.

Pierre Grussenmeyer received the B.Eng. degree in geodetic surveying and topography from the Institut National des Sciences Appliquées (INSA) de Strasbourg, Strasbourg Cedex, France, in 1984 and the Ph.D. degree in photogrammetry from the University of Strasbourg, Strasbourg Cedex (in relationship with the Institut Geographique National (IGN), Paris, France), in 1994.

From 1988 to 2004, he was an Associate Professor with INSA de Strasbourg. Since 2004, he has been a Professor with the Equipe Photogrammétrie et Géomatique, CNRS, INSA de Strasbourg, and the Head of the "Photogrammetry and Geomatics Group" of the UMR MAP 694 research center. His current research interests include close-range photogrammetry, architectural photogrammetry and laser scanning, visual and virtual models, and cultural heritage documentation.

Dr. Grussenmeyer has been a member of the International Society for Photogrammetry and Remote Sensing (ISPRS) since 1996. He has been the Treasurer and a member of the Board of the International Committee for Architectural Photogrammetry since 1999. He is also a Vice President of the Association Française de Topographie.
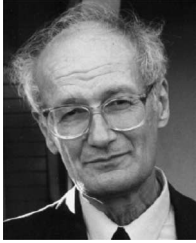
Vasile Buzuloiu (M'91–SM'05) received the M.S. and Ph.D. degrees in electronics from the University Politehnica Bucharest, Bucharest, Romania, in 1959 and 1980, respectively, and the M.S. degree in mathematics from "Universitatea Bucuresti," Bucharest, Romania, in 1971.

He is currently a Professor with the Department of Applied Electronics and Information Engineering, University Politehnica Bucharest. He also heads the Image Processing and Analysis Laboratory and is a Research Associate with CERN, Geneva, Switzerland. He also holds the title of Honorary Professor of the University Transilvania, Brasov, Romania (2001). Since 1994, he has held various positions of Invited Professor at French Universities (INSA de Lyon, Villeurbanne Cedex, ESIA-Université de Savoie, Annecy Cedex, Université de St. Etienne, St. Etienne, Université de Poitiers, Poitiers Cedex, INP de Toulouse, Toulouse Cedex, etc.). Since 1995, he has been the Director of the Spring International School "Multidimensional Signal Processing and Analysis: Methods, Algorithms, Technologies, Applications" which is organized yearly at the University Politehnica Bucharest. His research interests include mathematical modeling, statistical decisions, encryption, digital signal processing, image processing and analysis systems, and image processing applications.

Dr. Buzuloiu is a member of the International Society for Optical Engineering (SPIE), Color Group (Great Britain), and the Romanian Society for Applied Mathematics. He received the "Traian Vuia" Award of the Romanian Academy (1985) for the first digital image analysis system developed in Romania.

Irena Hajnsek received the Dipl. degree (with honors) from the Free University of Berlin, Berlin, Germany, in 1996 and the Ph.D. degree (with honors) from the Friedrich Schiller University of Jena, Jena, Germany, in 2001.

From 1996 to 1999, she was a Project Scientist with the German Aerospace Center (DLR), Microwaves and Radar Institute, Wessling. From 1999 to 2000, she was an EU Fellow with the Institut d'Electronique et de Telecommunications de Rennes, University of Rennes I, Rennes, France, and with Applied Electromagnetics (AEL), St. Andrews, U.K. In 2000, she joined again the German Aerospace Center, Microwaves and Radar Institute, SAR Technology Department. Since 2002, she has been leading the Polarimetric SAR Interferometry research group. In 2005, she was a Visiting Scientist at The University of Adelaide, Adelaide, Australia. She is responsible for the polarimetric science exploration of TerraSAR-X and the Coordinator of the TanDEM-X science team. Her current research interests include electromagnetic propagation and scattering theory, radar polarimetry, SAR and interferometric SAR data processing techniques, environmental parameter modeling, and estimation.

Dr. Hajnsek received the DLR science award in 2002.

Christian Andres received the Dipl. degree in information technology from the University of Applied Sciences Wiener Neustadt, Wiener Neustadt, Austria, in 2005.

In 2004, he joined the German Aerospace Center, Microwaves and Radar Institute, SAR Technology Department, Wessling, for the development of SAR signal processing algorithms for the Experimental Airborne SAR Sensor (E-SAR) and its successor F-SAR. His main field of activity was in the area of airborne SAR interferometry, geocoding, motion compensation, and differential SAR interferometry. His research interests include signal and image processing within distributed computer architectures.

Martin Keller received the M.S. degree in geophysics from the University of Karlsruhe, Karlsruhe, Germany, in 2000.

Afterward, he joined the Danish Defence Research Establishment in Copenhagen, Denmark, in the frame of the European TMR project (Training and Mobility of Young Researchers). Since 2001, he has been with the German Aerospace Center, Microwaves and Radar Institute, SAR Technology Department, Wessling. He is involved in the preparation and accomplishment of E-SAR measurement campaigns and in the processing of the recorded data.

Ralf Horn received the Dipl.-Ing. degree in electrical engineering, with major subjects in telecommunications and radio-frequency engineering, from Ruhr-Universitaet-Bochum, Bochum, Germany, in 1983.

He joined the German Aerospace Center (DLR), Microwaves and Radar Institute, SAR Technology Department, Wessling, in 1983. From 1983 to 1986, he was a Radar Engineer on the development of DLR's airborne experimental SAR system E-SAR, and later on, became a SAR Systems Engineer. In 1994, he was promoted as a Team Leader of the "Airborne SAR" group of the SAR Technology Department. His current responsibilities are mainly focused on the project management for the new DLR airborne SAR system F-SAR and on the management, coordination, and execution of DLR airborne SAR missions in Europe and abroad.